ARCHIVES OF ACOUSTICS
36, 4, 945–954 (2011)

DOI: 10.2478/v10168-011-0064-2

Thick Film Transducers for High Frequency Coded Ultrasonography

Andrzej NOWICKI[1], Marcin LEWANDOWSKI[1], Janusz WÓJCIK[1], Ryszard TYMKIEWICZ[1], Rasmus LOU–MOLLER[2], Wanda WOLNY[2], Tomasz ZAWADA[3]

(1) *Department of Ultrasound*
Institute of Fundamental Technological Research
Polish Academy of Sciences
Pawińskiego 5B, 02-106 Warszawa, Poland
e-mail: anowicki@ippt.gov.pl

(2) *InSensor A/S*
Hejreskovvej 18A, 3490 Kvistgaard, Denmark

(3) *Ferroperm Piezoceramics A/S*
Hejreskovvej 18A, 3490 Kvistgaard, Denmark

(*received July 5, 2011; accepted November 24, 2011*)

Recently a new technology of piezoelectric transducers based on PZT thick film has been developed as a response to a call for devices working at higher frequencies suitable for production in large numbers at low cost. Eight PZT thick film based focused transducers with resonant frequency close to 40 MHz were fabricated and experimentally investigated. The PZT thick films were deposited on acoustically engineered ceramic substrates by pad printing. Considering high frequency and nonlinear propagation it has been decided to evaluate the axial pressure field emitted (and reflected by thick metal plate) by each of concave transducer differing in radius of curvature – 11 mm, 12 mm, 15 mm, 16 mm.

All transducers were activated using AVTEC AVG-3A-PS transmitter and Ritec diplexer connected directly to Agilent 54641D oscilloscope. As anticipated, in all cases the focal distance was up to 10% closer to the transducer face than the one related to the curvature radius. Axial pressure distributions were also compared to the calculated ones (with the experimentally determined boundary conditions) using the angular spectrum method including nonlinear propagation in water. The computed results are in a very good agreement with the experimental ones. The transducers were excited with Golay coded sequences at 35–40 MHz. Introducing the coded excitation allowed replacing the short-burst transmission at 20 MHz with

the same peak amplitude pressure, but with almost double center frequency, resulting in considerably better axial resolution. The thick films exhibited at least 30% bandwidth broadening comparing to the standard PZ 27 transducer, resulting in an increase in matching filtering output by a factor of 1.4–1.5 and finally resulting in a SNR gain of the same order.

Keywords: transducers, thick film, high frequency ultrasound, pulse compression, Golay codes.

1. Introduction

High frequency (HF) ultrasonography is gaining increased interest in skin, eye and small animals imaging. However, an excessive attenuation of ultrasound at HF limits the range of the available frequencies, considering the permissible peak pressure of the probing beam. Our motivation was to develop the dedicated transducers exhibiting wide-bandwidth behavior and enabling transmission of wide-band coded probing pulses with peak pressure not exceeding the acceptable levels. The TAWE simulation software (Wójcik *et al.*, 2006) was used to solve the field distribution for investigated transducers.

2. Materials and methods

The developed new technology of piezoelectric transducers based on PZT thick film devices have already been successfully commercialized by InSensor A/S. Since the PZT thick film transducers are relatively new devices existing on the market special attention must be put into the characterization methods that take into account some specific features of these transducers. The backing material (InSensor SU37) is based on Ferroperm composition Pz37, a porous engineered structure version of PZT. The backing is also used as substrate for the thick film

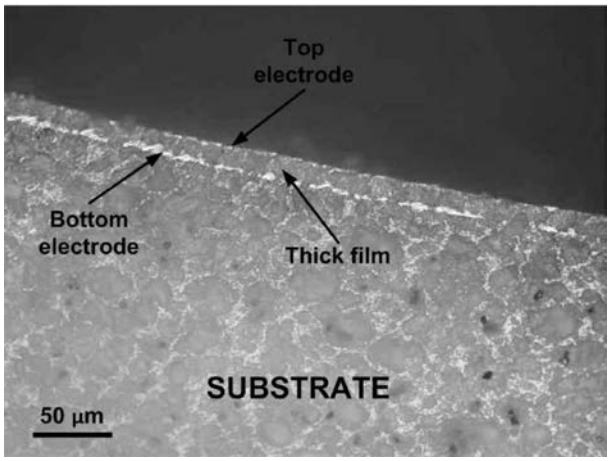

Fig. 1. Cross-section of a focused thick film.

and will therefore be referred to as the substrate. The pores in the substrate give rise to a significant surface roughness. Since the surface roughness is comparable to the thickness of the thick film, a smoothing layer is printed before deposition of the bottom electrode layers. In order to deposit thick film layers on a curved surface, the technology of pad printing was used.

2.1. Pad printing process

In order to deposit thick film layers on a curved surface, the technology of pad printing has been implemented. For this purpose, paste prepared for traditional screen-printing, with some modification of the rheological properties is used. An illustration of the pad printing technique is given in Fig. 2. The printing setup consists of a silicone rubber pad, a steel cliché, a doctor blade and a substrate. The paste is flooded onto the etched pattern in the cliché and the doctor blade removes excess paste. Hereafter, the paste is transferred to the substrate by a silicon pad.

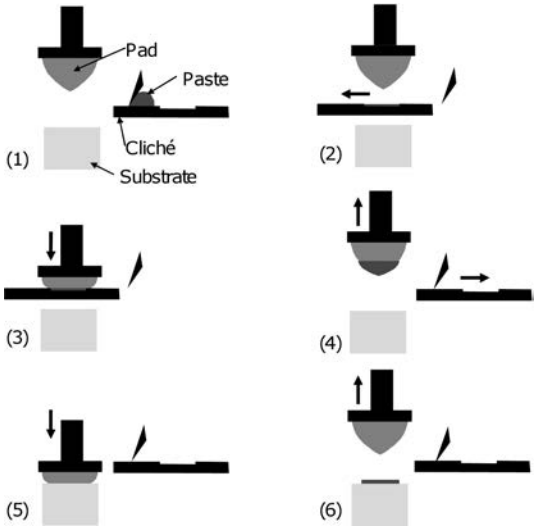

Fig. 2. Illustration of the technology of pad printing.

After printing, the organic vehicle is dried off in a ventilated oven at about 100°C. Several layers of PZT are printed in order to obtain the desired thickness of the film. For a fired thickness of about 20 μm 15 layers of PZT is printed in this manner. After printing of all the layers, the film is sintered at 850°C for one hour. For bottom and top electrodes, commercial gold and silver pastes are used, respectively. Since the pad is flexible, the thick film can be deposited onto substrates with complex topography. However, the flexibility of the pad can also cause a distortion of the pattern. For simple structures such as circles, this distortion is not a problem, but for more complicated structures and structures,

where different patterns have to be aligned to each other; this must be taken into consideration. The samples are poled in air at 150°C with an applied field of 10 kV/mm for 10 minutes.

The paste prepared for the traditional screen printing can be used for pad printing as well, however, after some modification of the rheological properties.

3. Measurements

Eight PZT thick film based disk type focused transducers with 2 mm diameter were investigated. The investigated transducers were mounted on SU37 support material. The backscattering echoes from the backing material were kept at the sufficiently low level to prevent the real echoes from the remaining clutter (below −70 dB).

Next, the transducers were activated by 70 Vpp amplitude, 4 ns pulses generated by AVTECH AVG-3A-PS Pulser (Ogdensburg, NY, USA). The front of the transducer was immersed in water and the echo from the flat steel reflector was recorded. The FFT spectra of the received echoes are presented in Fig. 3. Admittance of the transducer measured on the Agilent 4395A Network Analyzer is presented in Fig. 4.

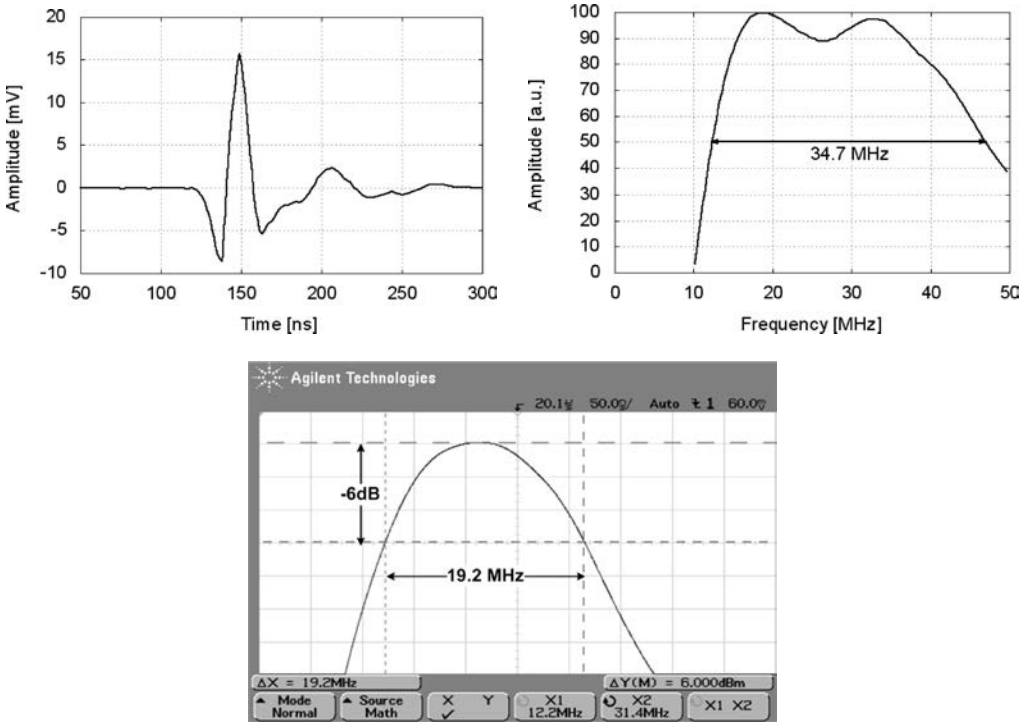

Fig. 3. (top left) ultrasonic pulse and (top right) bandwidth for the thick-film transducer; (bottom) bandwidth for the Pz27 transducers.

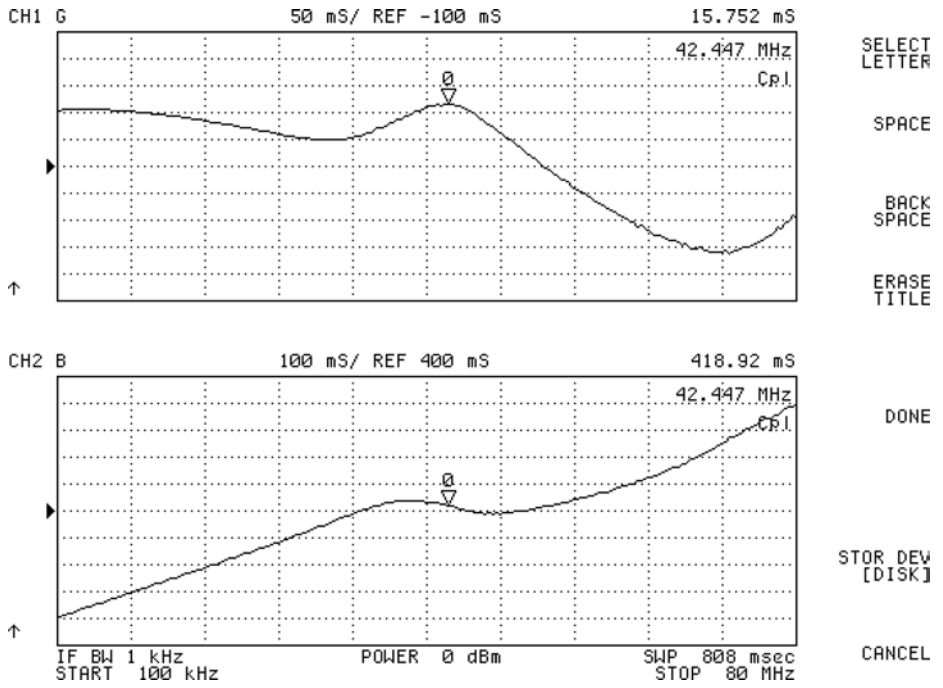

Fig. 4. Thick-film transducer admittance plot measured on Agilent 4395A Network Analyzer.

Clearly, as can be seen in Fig. 3, the relative bandwidth of the thick film transducer is larger than the bandwidth of the bulk PZT. The measurements of the echoes were done with electrical matching circuitry connected to the transducer. The transducers were also excited by one or two period sine bursts generated by the transmitter from the high frequency ultrasonic scanner designed for the skin imaging. For the focused transducer, additional measurements of ultrasonic field were performed by means of the Schlieren imaging device and the ultrasonic scanning microscope (SAM).

The investigated transducer was mounted in the SAM lens holder instead of a standard microscope head, so the transducer was operating in transmitting – receiving mode using e SAM's electronics. The field emitted by the transducer was probed with a small spherical reflector (100 μm diameter). This reflector moved mechanically in the C-scan cross-section, scanning "pixel by pixel" the transducer field at the constant distance from the transducer. The pulses reflected from a ball-like reflector were next captured by the transducer and send to the SAM receiver. The amplitude of echoes was used to control the brightness of the pixels on SAM's monitor. After completing the scanning, the image corresponding to pressure field distribution was created and stored. The measurements were done in focal plane. The scanning area was 0.4 mm × 0.4 mm. The image obtained in focal plane (11 mm) shows perfect focusing properties of the transducer, Fig. 5.

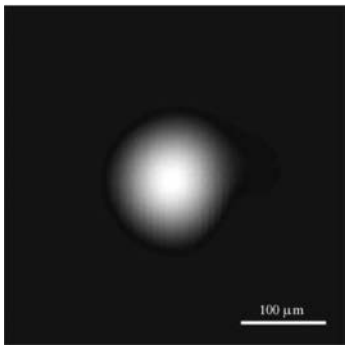

Fig. 5. Pressure field distribution at the focal plane.

In the next step the axial and lateral variation of the pressure field were measured. Two different set of measurements were done. For the axial field the plane perfect reflector was used and the echo signal was recorded representing the product of the transmitted and received fields. For lateral measurements the needle like reflector (small, 40 micrometers in diameter ball) was used. It was shown, that in all cases the measured focal position was shifted toward the transducer face by about 10%, from 1 to 1.5 mm.

The experimentally measured pulse shape was next used as the driving pressure pulse at the numerical simulation. The spectral shift due to the attenuation in water was accounted. The only difference was in neglecting the residual "ringing" tail.

Theoretical analysis of the nonlinear scalar wave equation, describing the propagation of sound, made it possible to develop a very efficient numerical code solving this equation in the PC domain for one-side boundary problems. The new method applied for axially symmetrical (2D) problems makes the calculation times at least several times shorter for weak nonlinearities. The developed numerical code provides information, which make it possible to obtain all stationary and dynamic characteristics of the field generated by such a probe (but also by linear arrays) and especially its time-spatial (4D) visualization (Wójcik *et al.*, 2006; 2008a; 2008b). In this way such a solver, besides of pure scientific applications of solving equations of nonlinear acoustics, can be used as a basic tool to support and rationalize the process of design of the probe as a source of the acoustic field with finite amplitudes. It allows us 1) to test the scientific ideas for possible practical applications; 2) to evaluate the materials; 3) to choose working conditions to optimize the beam shape; 4) to determine the influence of technological defects on the distribution of the acoustic field; 5) to identify the properties of transmitting probes by comparison of measured and computed fields; 6) calibration of hydrophones; 7) to determine the secondary effects – positive like hyperthermia and negative thermal effects, mechanical effects – determination of safe radiation doses.

For axially symmetrical disturbances (2D+time), generated by circular sources, the above mentioned problems can be and are solved by means of codes used in PC environments on the basis of methods known since many years (CHRISTOPHER, PARKER, 1991; KUZNETSOV, 1970). In such a case the expanding power of processors have a distinct effect on the performance of these solvers.

The comparison between the measured and simulated data on one hand proved the exceptionally good performance of all investigated transducers but also showed the validity of the numerical algorithm. Assuming the validity of computation for other focused transducers in similar frequency range and of similar geometrical dimensions one can skip the rather tedious field measurements, especially when hydrophone active field is in range of the wave length. The experimental and numerical data for transducer No. 3 and No. 5 are compared in Figs. 6 and 7. One can appreciate the good agreement between both data.

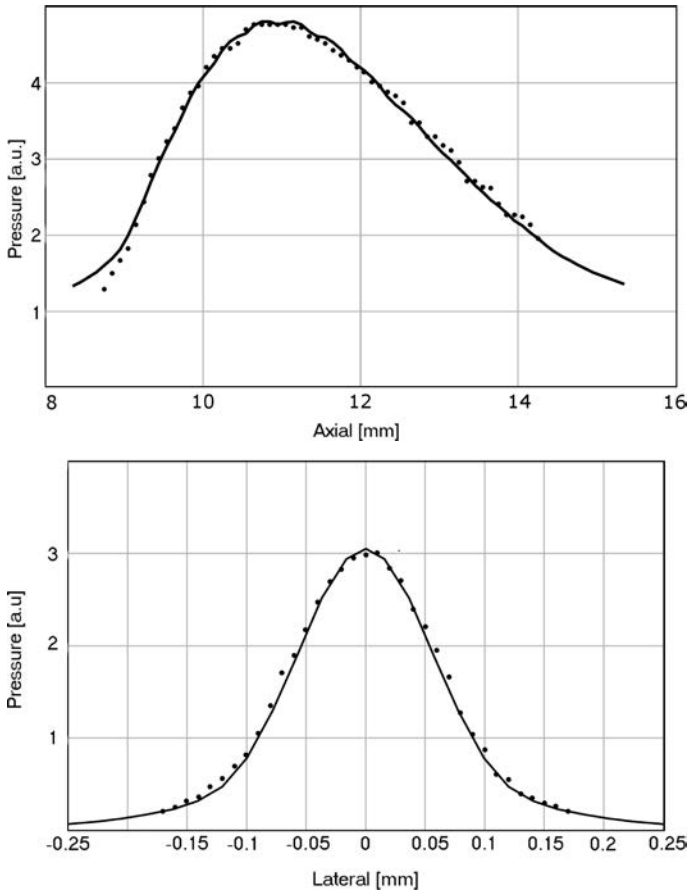

Fig. 6. (top) Ultrasonic measured (dots) and computed axial pressure (solid line); (bottom) later pressure distribution for transducer No. 3 – measured (dots) and computed (solid line). Focus depth = 11 mm, $f = 40$ MHz.

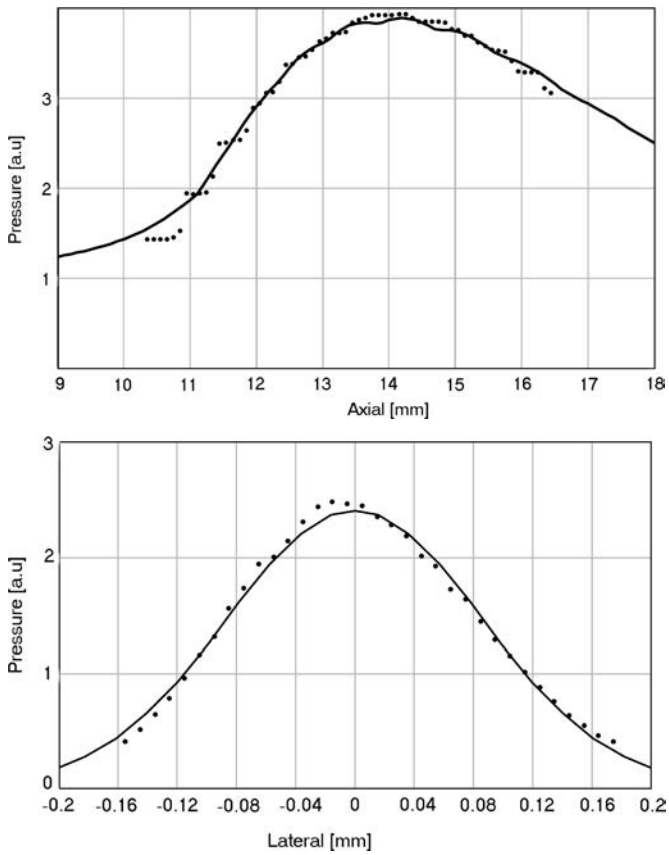

Fig. 7. (top) Ultrasonic measured (dots) and computed axial pressure (solid line); (bottom) later pressure distribution for transducer No. 5 – measured (dots) and computed (solid line). Focus depth = 16 mm, f = 40 MHz, the measured width (−6 dB) of the focal spot was equal to 150 μm.

The scanner and the mechanical wobbling probe were specially designed for this project. The innovative part of the scanner included fully arbitrary excitation sequences from short 1/2 period bursts up to 1024 points synthesized Golay coded transmissions (Lewandowski, Nowicki, 2008; Nowicki *et al.*, 2006).

Golay complementary sequences are pairs of binary codes belonging to a bigger family of signals called complementary pairs, which consists of two codes of the same length n, whose auto-correlation functions have side-lobes equal in magnitude but opposite in sign. Summing them up results in a composite auto-correlation function with a peak amplitude equal to $2n$ and zero level side-lobes. We have used the code pair of the following structure

$$\text{Code 1} = \{1, 1, 1, -1, 1, 1, -1, 1, 1, 1, 1, -1, -1, -1, 1, -1\}$$

and

$$\text{Code 2} = \{1, 1, 1, -1, 1, 1, -1, 1, -1, -1, -1, 1, 1, 1, -1, 1\},$$

where +1 corresponds to the positive phase of the sine period and −1 corresponds to the opposite phase ($+\pi$) respectively. The example of the 16 bit 35 MHz Golay code before and after the decompression is presented in Fig. 8. The ultrasonic images of the skin structure with cellulite, recorded in the clinical conditions are presented in Fig. 9.

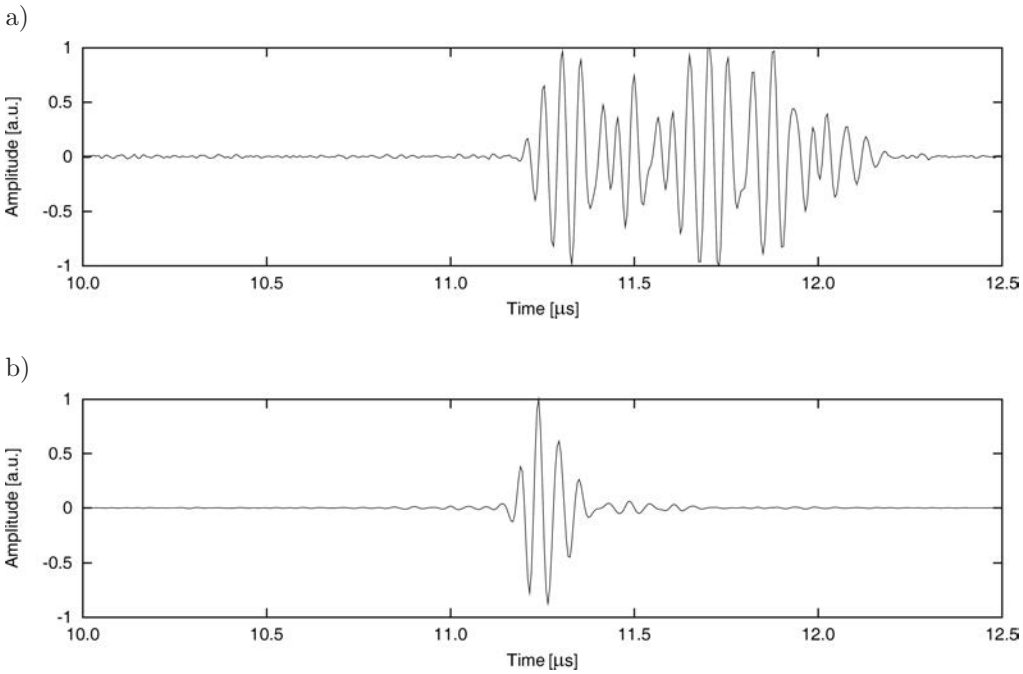

Fig. 8. 16 bit Golay code 1 before and after the decompression. Ultrasonic echo reflected from the steel plate.

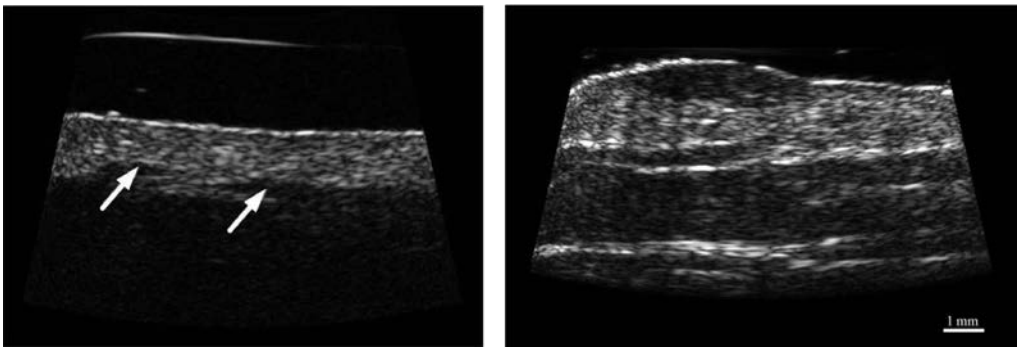

Fig. 9. Ultrasonic image obtained with a thick film transducer focused at 11 mm, excitation 16 bit, 35 MHz Golay code; (left) cellulite – solid arrows show the sites of the subcutaneous tissue ingrowing into dermis; (right) skin hemangioma.

4. Conclusions

The novel thick film focused transducers of the 20 μm layer thickness operated at frequencies 30–40 MHz, were investigated. They exhibited extremely wide bandwidth (over 80% when appropriately driven) and good efficiency (especially after adding quarter wave matching layers), resulting in excellent superficial tissue imaging.

Introducing the coded excitation allowed replacing the short-burst transmission with the same peak amplitude pressure, but using almost twice the center frequency, resulted in considerably better axial resolution. The important factor for coded transmission/reception is the matching of the transducer bandwidth with the one of the coded signal. The thick films exhibited at least 30% bandwidth broadening, resulting in an increase in matching filtering output by a factor of 1.4–1.5 and finally resulting in a SNR gain of the same order.

The preliminary clinical studies of the skin lesions and cellulites were performed proving the superiority of the thick films transducers over the bulk material in terms of the extended bandwidth and efficiency resulting in increased resolution and deeper penetration depth when working in the coded regime.

References

1. Christopher P., Parker K. (1991), *New approaches to nonlinear diffractive field propagation*, J. Acous. Soc. Am., **90**, 488–499.
2. Kuznetsov V.P. (1970), *Equations of nonlinear acoustics*, Akust. Zh., **16**, 548–553.
3. Lewandowski M., Nowicki A. (2008), *High frequency coded imaging system with RF software signal processing*, IEEE Trans. Ultrason. Ferroelectr. Freq. Control, **55**, 8, 1878–1882.
4. Nowicki A., Klimonda Z., Lewandowski M., Litniewski J., Lewin P.A., Trots I. (2006), *Comparison of sound fields generated by different coded excitations – experimental results*, Ultrasonics, **44**, 1, 121–129.
5. Wójcik J., Nowicki A., Lewin P.A., Bloomfield P.E., Kujawska T., Filipczynski J. (2006), *Wave envelopes method for description of nonlinear acoustic wave propagation*, Ultrasonics, **44**, 3, 310–329.
6. Wójcik J., Kujawska T., Nowicki A., Lewin P.A. (2008), *Fast prediction of pulsed nonlinear acoustic fields from clinically relevant sources using time-averaged wave envelope approach: Comparison of numerical simulations and experimental results*, Ultrasonics (Elsevier), **48**, 8, 707–715.
7. Wójcik J., Kujawska T., Nowicki A. (2008), *Pulsed nonlinear acoustic fields from clinically relevant sources; numerical calculations and experimental results*, Archives of Acoustics, **33**, 4, 565–572.